

Analysis of Temperature Effects on Tension Infiltrometry of Low Permeability Materials

Paolo Castiglione, Peter J. Shouse,* Binayak P. Mohanty, and Martinus Th. van Genuchten

ABSTRACT

Tension infiltrometers have become popular for in situ measurement of the near-saturated hydraulic conductivity as a function of the soil water pressure head. Unfortunately, fluctuating ambient temperatures can cause dramatic pressure variations due to the presence of confined air inside the infiltrometer, thereby affecting the intended pressure head to be applied to the soil surface and hence also the measured infiltration rate. This is especially true for low infiltration rates and long equilibration times typical of low permeability materials, including unsaturated fractured rock. We developed a model to analyze the effects of temperature changes on the static pressure of the confined air volume within tension infiltrometers. The model was tested using several prototype infiltrometer designs in a computer-controlled variable-temperature room. Experimental results confirmed the model simulations. For example, predicted and measured changes in the pressure head in one experiment were 11.2 and 12.5 cm following a change of 18.5°C in the temperature. Using the model, we were able to optimize several infiltrometer designs that significantly reduced the undesired effects of temperature on tension infiltration results.

TENSION INFILTRMETERS (Perroux and White, 1988) are now widely used to characterize field soil infiltration rates and infiltration parameters such as the sorptivity and the saturated or near-saturated hydraulic conductivity (e.g., Perroux and White, 1988; Clothier and White, 1981). They are especially useful for soils that display preferential flow (Lin and McInnes, 1995; Jarvis and Messing, 1995; Mohanty et al., 1996, 1997; Bagarello et al., 2000). Others have used tension infiltration to characterize the size, continuity, and transport efficacy of soil macropores (Watson and Luxmoore, 1986; Wilson and Luxmoore, 1988). By making specific assumptions about the shape of the wetting front, it is possible to obtain the hydraulic conductivity corresponding to the applied tension (e.g., Wooding, 1968) or additional information about the soil hydraulic functions from numerical or analytical analyses of cumulative infiltration data (Simunek et al., 1998; Vandervaere et al., 2000; Schwartz and Evett, 2002).

The popularity of tension infiltrometers is in large part due to the fact they are portable, easy to use, and relatively robust for field applications. Typically, a tension infiltrometer consists of a coupled Mariotte tower and reservoir tower connected to a permeable porous supply

disk having an air entry pressure of approximately -25 cm of water, contact material, and a ring for holding the contact material and leveling the supply disk (Fig. 1). As water infiltrates across the soil surface, an equal volume of air enters the reservoir through Tubes B and C. The procedure establishes a constant negative pressure at the soil surface, which can be adjusted by manipulating Tube B in the Mariotte tower. The infiltration rate is measured (often by means of a pressure transducer) from water volume changes in the reservoir tower (Perroux and White, 1988; Ankeny et al., 1988).

An important feature of a well-designed infiltrometer is the presence of constant pressure at the soil surface as the infiltration proceeds and the reservoir tower empties. Unfortunately, this feature can generally be attained only when all environmental conditions remain constant. Because of extremely low infiltration rates and associated long equilibration times, environmental factors normally neglected during tests in soils may not be negligible for tests on low permeability materials such as unsaturated fractured rock (Castiglione et al., 2005). Fluctuating ambient temperatures, in particular, can cause dramatic variations in the applied pressure, thus affecting measurements of infiltration. This is due to the presence of air pockets inside the reservoir and Mariotte towers (Fig. 1) that are not completely free to expand or contract. This phenomenon is analogous to the widely observed pressure changes in tensiometers responding to diurnal temperature fluctuations (Richards et al., 1937; Butters and Cardon, 1998; Warrick et al., 1998).

Unlike with tensiometers, observations of temperature induced pressure fluctuations in the Mariotte tower of tension infiltrometers have not been made, mostly because measurements in soils typically last for only one to several hours or less. Since high infiltration rates lead to short equilibration times, the entire test generally will not last long enough to experience significant temperature variations. Our experience indicates that temperature effects become a major concern for low permeability systems, such as certain clay soils and landfill caps or liners and unsaturated fractured rock formations. Such low permeability media are different from most soils in that measurements may easily take from several days (clays) to several months (rock formations) to reach a steady-state flow process. Accurate tension infiltrometer measurements in these situations require the use of an infiltrometer system that minimizes the effects of temperature fluctuations on the Mariotte and reservoir tower pressures.

Our objectives in this study were to analyze the effects of temperature and pressure fluctuations in both a single Mariotte tower and a complete tension infiltrometer system during static (no-flow) conditions. We provided a relatively simple model to predict pressure variations as a function of temperature and then used the model to de-

P. Castiglione, Land Resources and Environmental Science Dep., Montana State Univ., 334 Leon Johnson Hall, Bozeman, MT 59717; P.J. Shouse and M.Th. van Genuchten, USDA-ARS, George E. Brown, Jr. Salinity Laboratory, 450 W. Big Springs Rd., Riverside, CA, 92507; B. Mohanty, Dep. of Biological and Agricultural Engineering, 301 Scoates Hall, Texas A&M Univ., College Station, TX 77843-2117. Received 17 Sept. 2004. *Corresponding author (pshouse@ussl.ars.usda.gov).

Published in Vadose Zone Journal 4:481–487 (2005).

Original Research Paper

doi:10.2136/vzj2004.0134

© Soil Science Society of America

677 S. Segoe Rd., Madison, WI 53711 USA

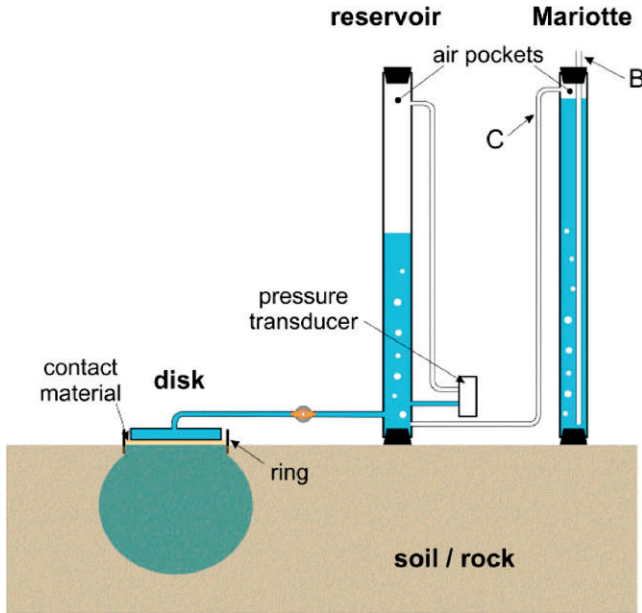


Fig. 1. Schematic of typical tension infiltrometer.

use a measurement strategy that minimizes temperature effects. Since the model holds for no-flow conditions, the predicted pressure changes should reflect a worst-case scenario of the effects of temperature on tension infiltrometer performance.

ANALYSIS OF TEMPERATURE EFFECTS Mariotte Tower

Before discussing a complete tension infiltrometer system, let us first analyze the simple case of a single Mariotte tower. Consider for this purpose the Mariotte tower depicted in Fig. 2a, and assume that Valve A is being closed while air is bubbling from Tube B. The closure of Valve A will interrupt the air flux and “freeze” the initial pressure distribution (subscript “i”), as shown in Fig. 2a. The question arises, how will this system respond to an increase in temperature? Since the air pocket in the top of the tower cannot expand freely, its pressure will tend to increase. The increasing pressure will push water into Tube B until a new equilibrium is achieved, as shown in Fig. 2b, with the position of the water meniscus determining the final pressure distribution (subscript “f”) within the Mariotte tower. In particular, the pressure change (ΔP) in the air pocket is given by

$$\Delta P = P_f - P_i = \Delta a + k \quad [1]$$

which indicates that ΔP is the sum of the vertical air pocket expansion (Δa) and the vertical displacement of the water meniscus (k) into Tube B. If s is the cross-sectional area of Tube B and S the difference between the cross-sectional areas of the Mariotte tower and Tube B, then mass conservation requires that k and Δa are related through

$$k = \Delta a \frac{S}{s} \quad [2]$$

The pressure (P), volume (V), and temperature (T)

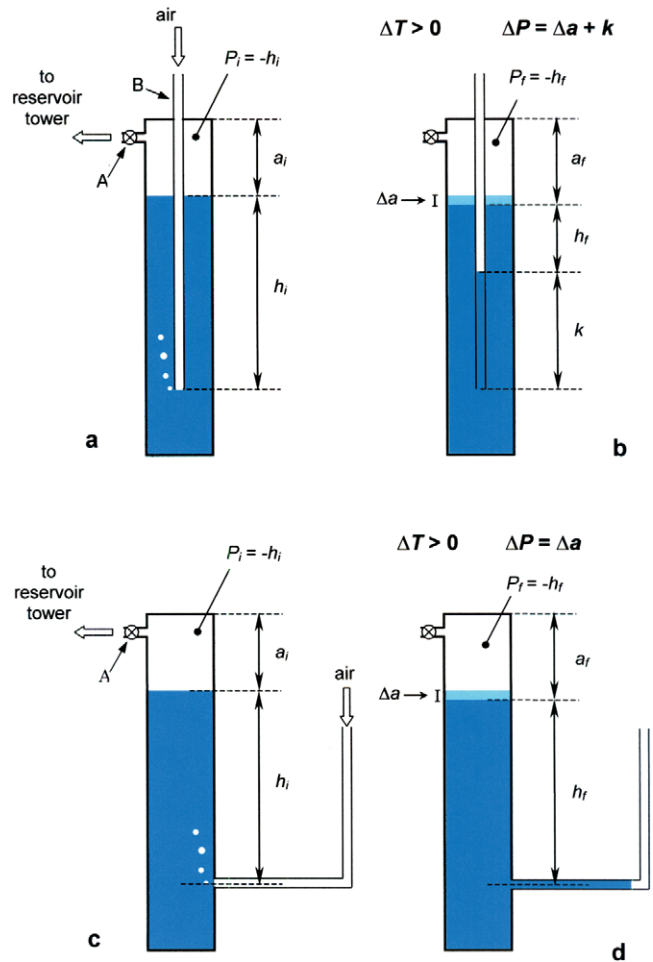


Fig. 2. Schematic of conventional Mariotte tower under (a) flowing conditions, (b) static conditions after increased ambient temperature and modified Mariotte tower under (c) flowing conditions and (d) static conditions after increased ambient temperature.

of the air pocket in the Mariotte tower are related by the ideal gas law:

$$PV = nRT \quad [3]$$

where n is the mass of air in moles, and R the gas constant ($8.3145 \text{ J mol}^{-1} \text{ K}^{-1}$). Assuming that the air mass does not change during an expansion of the air pocket, we can write

$$\frac{P_i V_i}{T_i} = \frac{(P_i + \Delta P)(V_i + \Delta V)}{(T_i + \Delta T)} = nR = \text{const} \quad [4]$$

where subscript “i” indicates the initial state as before, and Δ refers to small changes in P , V , and T from the initial state. Since $V_i = S a_i$ and $\Delta V = S \Delta a$, Eq. [4] can be rearranged to give

$$P_i a_i \left(1 + \frac{\Delta T}{T_i} \right) = (P_i + \Delta P)(a_i + \Delta a) \quad [5]$$

which on expansion simplifies to

$$a_i P_i \frac{\Delta T}{T_i} = \Delta a P_i + a_i \Delta P + \Delta a \Delta P \quad [6]$$

Using Eq. [2] to eliminate k from Eq. [1] yields

$$\Delta a = m\Delta P \quad [7]$$

where

$$m = \frac{s}{S + s} = \frac{\varepsilon}{1 + \varepsilon} \quad [8]$$

in which $\varepsilon = s/S$. Substituting Eq. [7] into Eq. [6] now leads to the following second-order equation in ΔP :

$$m\Delta P^2 + (mP_i + a_i)\Delta P - a_iP_i \frac{\Delta T}{T_i} = 0 \quad [9]$$

Only the positive root of Eq. [9] is physically meaningful. Given the initial values P_i , a_i , and T_i , and the geometric characteristic of the Mariotte tower (embedded in m), Eq. [9] gives the change in pressure, ΔP , corresponding to an increase in temperature, ΔT .

Before continuing, we first note that in a Mariotte tower the pressure distribution is uniquely determined by the position of the water meniscus in Tube B (the higher the meniscus, the higher the pressure), consistent with the hydrostatic condition given by Eq. [1]. The minimum pressure for the system occurs for the equilibrium condition depicted in Fig. 2a, where the water meniscus is at its lowest position. Assume now that the system, originally as shown in Fig. 2a, did undergo a temperature increase ($\Delta T_1 > 0$) and reached a new equilibrium as in Fig. 2b. If, starting from this new condition (Fig. 2b), a temperature reduction occurs ($\Delta T_2 < 0$), then the air pocket will shrink and its pressure will decrease, together with the position of the meniscus in Tube B. Clearly, if $|\Delta T_2| = |\Delta T_1|$, the original conditions shown in Fig. 2a will be reestablished. However, any further temperature reductions beyond the minimum pressure condition (Fig. 2a) will no longer lead to further changes in the pressure or volume of the air pocket, but rather will cause additional air to enter the system in the form of bubbles from Tube B. In actuality, the additional temperature drop will be compensated by an increase in the n term (i.e., of the air mass) of Eq. [2]. The additional mass of air (Δn) that enters the system can be calculated from Eq. [3], with P and V constant:

$$n_i T_i = (n_i + \Delta n)(T_i + \Delta T) = \text{const} \quad [10]$$

In summary, when the Mariotte tower undergoes cyclic temperature changes (e.g., diurnal temperature fluctuations) the pressure will vary according to the temperature, with the lowest temperature determining the maximum amount of air entering the system.

Tension Infiltrator

The response of the tension infiltrator to temperature variations is similar to that of a single Mariotte tower. Variations in pressure within the system result from interactions between the volumes of confined air in the reservoir (subscript "R") and Mariotte (subscript "M") towers (Fig. 3). Let us assume that the pressure distribution in the system initially is as shown in Fig. 3a, and that the water flux through the disk (and therefore the air flow through Tubes B and C) is interrupted. The system will then respond in two different ways to increased temperature, as discussed below.

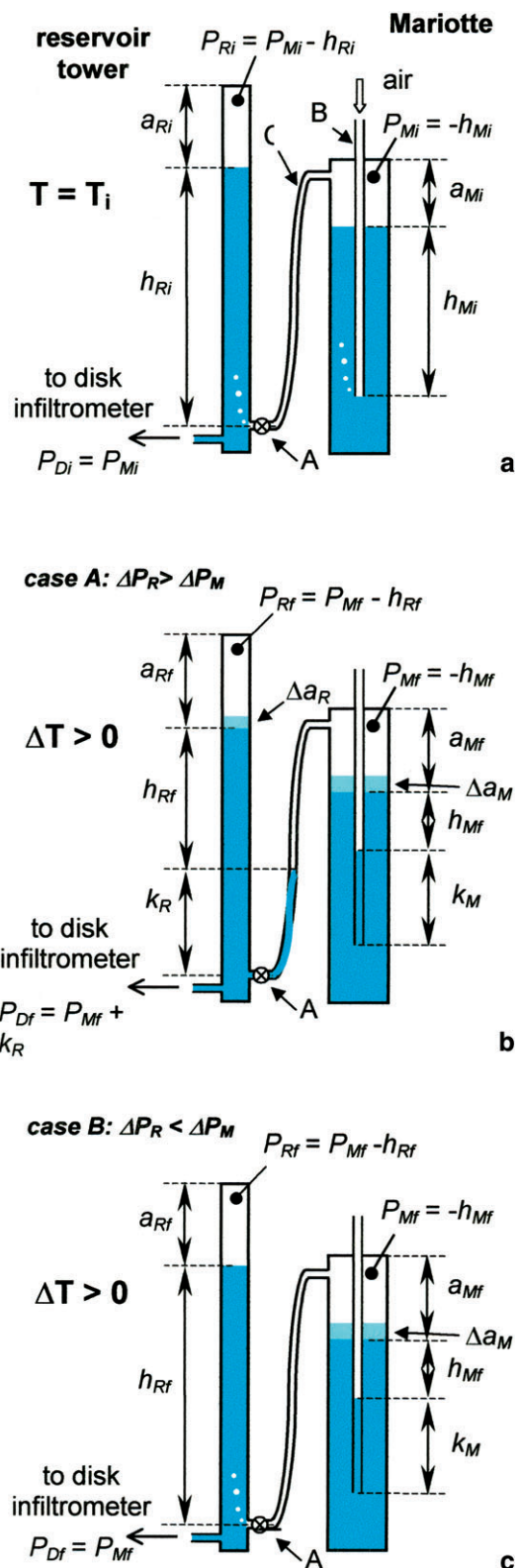


Fig. 3. (a) Schematic of typical Mariotte and reservoir system under flowing conditions (top), as well as for (b) static conditions with increasing ambient temperature for reservoir pressures greater than the Mariotte pressure (Case A) and (c) less than the Mariotte pressure (Case B).

Case A: $\Delta P_R > \Delta P_M$

If the pressure change in the reservoir air pocket (ΔP_R) is greater than that in the Mariotte air pocket (ΔP_M), water will be pushed from the reservoir into the interconnecting Tube C (Fig. 3b). Very much analogous to the description in the previous section, the pressure distribution at equilibrium is given by the set of equations:

$$\left\{ \begin{array}{l} \Delta P_R = k_R + \Delta a_R + \Delta P_M \\ \Delta P_M = k_M + \Delta a_M \\ \Delta a_R = \frac{s_C}{S_R} k_R = \varepsilon_R K_R \\ \Delta a_M = \frac{s_B}{S_M} k_M = \varepsilon_M k_M \\ \frac{P_{Mi} V_{Mi}}{T_i} = \frac{(P_{Mi} + \Delta P_M)(V_{Mi} + S_M \Delta a_M - s_B k_R)}{T_i + \Delta T} \\ \frac{P_{Ri} a_{Ri}}{T_i} = \frac{(P_{Ri} + \Delta P_R)(a_{Ri} + \Delta a_R)}{T_i + \Delta T} \end{array} \right. \quad [11]$$

where s_B and s_C represent the cross-sectional areas of Tubes B and C, respectively, S_M is the difference between the cross-sectional area of the Mariotte tower and s_B , and S_R is the difference between the cross-sectional area of the reservoir and s_C . The meaning of the remaining symbols in Eq. [11] is evident from Fig. 3. The first two equations of Eq. [11] express hydrostatic equilibrium in the reservoir and Mariotte towers, respectively. The third and fourth equations account for conservation of mass, while the last two equations represent the ideal gas law as applied to the volumes of confined air in the two towers. Notice that the initial volume of air subject to expansion in the Mariotte (V_{Mi}) includes Tube C. Also the third equation of Eq. [11] assumes that Tube C is perfectly vertical, while ignoring any contribution of the short horizontal segment containing Valve A. Similarly, as before leading to Eq. [9], the system of equations given as Eq. [11] can be reduced to a system of two second-order equations of the form (details omitted here):

$$\left\{ \begin{array}{l} \left(\frac{S_M}{S_R} m_M + m_R \right) \Delta P_M^2 + \\ \left[\frac{S_M}{S_R} m_M P_{Mi} + \frac{V_{Mi}}{S_R} - m_R (\Delta P_R - P_{Mi}) \right] \\ \Delta P_M - P_{Mi} \left(m_R \Delta P_R + \frac{V_{Mi}}{S_R} \frac{\Delta T}{T_i} \right) = 0 \\ m_R \Delta P_R^2 + (m_R P_{Ri} + a_{Ri} - m_R \Delta P_M) \\ \Delta P_R - P_{Ri} \left(m_R \Delta P_M + a_{Ri} \frac{\Delta T}{T_i} \right) = 0 \end{array} \right. \quad [12]$$

where

$$m_M = \frac{\varepsilon_M}{1 + \varepsilon_M} \quad \text{and} \quad m_R = \frac{\varepsilon_R}{1 + \varepsilon_R} \quad [13]$$

As before, only the positive roots of Eq. [12] provide a physically meaningful estimate of the pressure change ΔP_M in response to a temperature change of ΔT .

Case B: $\Delta P_R < \Delta P_M$

If the pressure change in the Mariotte tower (ΔP_M) is greater than that in the reservoir tower (ΔP_R), air will be pushed (in the form of bubbles) from the Mariotte air pocket into the reservoir so that, at equilibrium, the system is as shown in Fig. 3c. The final pressure distribution is given by the system of equations:

$$\left\{ \begin{array}{l} P_{Mi} V_{Mi} = m_M R T_i \\ P_{Ri} \Sigma_R a_{Ri} = n_R R T_i \\ (P_{Mi} + \Delta P_M)(V_{Mi} + S_M \Delta a_M) = (n_M - \Delta n) R (T_i + \Delta T) \\ (P_{Ri} + \Delta P_R) S_R a_{Ri} = (n_R + \Delta n) R (T_i + \Delta T) \\ \Delta P_M = \Delta P_R \\ \Delta a_M = m_M \Delta P_M \end{array} \right. \quad [14]$$

where Δn is the mass of air transferred from the Mariotte tower to the reservoir. The first four equations of Eq. [14] express the ideal gas law applied to the volumes of confined air in the reservoir and Mariotte towers, respectively, for both the initial conditions (first and second equations) and the final conditions (third and fourth equations). The fifth equation of Eq. [11] results from the hydrostatic distribution, while the last equation again represents mass conservation analogous to Eq. [7]. The above system of equations can be reduced by repeated substitution to the following second-order equation:

$$\Sigma_M m_M \Delta P_M^2 + (S_M m_M P_{Mi} + V_{Mi} + S_R a_{Ri}) \Delta P_M - (V_{Mi} P_{Mi} + S_R a_{Ri} P_{Ri}) \frac{\Delta T}{T_i} = 0 \quad [15]$$

To determine the exact temperature response of the tension infiltrometer (i.e., which of the above two scenarios will occur), it is convenient to assume that the process proceeds in two successive phases. Initially the system is as shown in Fig. 3a, but with the Mariotte tower disconnected from the reservoir tower (Valve A closed). Upon a temperature increase ($\Delta T > 0$), the pressure in both air pockets increases. Since there is no interaction during this intermediate phase (subscript "int"), the changes in pressure in the reservoir and Mariotte towers are given by

$$\Delta P_{R,int} = P_{Ri} \frac{\Delta T}{T_i} \quad [16]$$

and

$$\left\{ \begin{array}{l} S_M m_M \Delta P_{M,int}^2 + (V_{Mi} + m_M S_M P_{Mi}) \Delta P_{M,int} - \\ P_{Mi} V_{Mi} \frac{\Delta T}{T_i} = 0 \end{array} \right. \quad [17]$$

respectively. Note that Eq. [17] is identical to Eq. [9], with the only difference being that the initial air volume now includes Tube C. Next, on opening Valve A, water will either move into Tube C (Fig. 3b) if $\Delta P_{R,int} > \Delta P_{M,int}$, or air will bubble into the reservoir tower (Fig. 3c) if $\Delta P_{R,int} < \Delta P_{M,int}$. The final pressure distribution of this Phase 2 can be obtained by solving the system of equa-

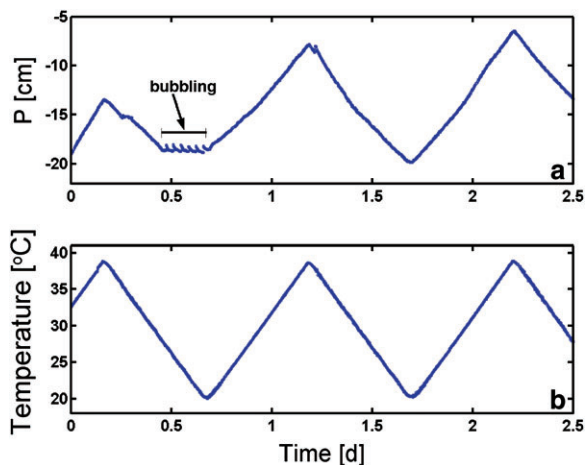


Fig. 4. Observed Mariotte pressure variations (P) as affected by imposed ambient temperature fluctuations (T) under no-flow conditions in controlled temperature room.

tions given by Eq. [12] (if $\Delta P_{R,int} > \Delta P_{M,int}$) or Eq. [15] (if $\Delta P_{R,int} < \Delta P_{M,int}$). Note that the system of equations given as Eq. [12] is nonlinear, and hence must be solved iteratively. The system is most conveniently solved using the intermediate pressure changes of Eq. [16] and [17] as initial values; the solution then usually converges within two or three iterations.

The derivations above are for increasing temperatures. The response to cooling is similar to that of a single Mariotte tower in that the pressure drops until the water menisci in tubes B and C are at their lowest positions, at which time additional air will enter the system (bubbles) and no further reductions in the pressure take place.

VERIFICATION OF PROCEDURE

The above analytical model (Eq. [12]) for quantifying the effects of temperature fluctuations on pressure distributions was tested during static (zero infiltration) conditions by placing the tension infiltrometer on an impermeable surface. The experiment was performed in a computer-controlled variable-temperature room that was programmed for seven diurnal temperature cycles (Fig. 4) of about 20°C involving 12 h of heating (20 – 40°C), followed by 12 h of cooling (40 – 20°C). We used a Mariotte tower of the type shown in Fig. 1, made of acrylic tubing 3.8 cm (1.5 inches) i.d. and 5.1 (2 inches) o.d. Rubber stoppers were sealed into the ends of the Mariotte tower using high temperature RTV sealant (an automotive cooling system sealant), after which the tower was pressure tested to 20.7 kPa (3 psi). We subsequently instrumented the tower with a calibrated, temperature-compensated pressure transducer (with a temperature compensation range of 0 to 50°C) to measure the pressure inside the air space in the top portion of the Mariotte tower.

Room temperatures and Mariotte tower air space pressures were measured for 3 d using an automatic data logger with a 30-s data acquisition interval. We started the experiment when the room and Mariotte temperatures were approximately 33°C . The Mariotte tower was sealed such that we could observe air being released (bub-

bling) from the Mariotte tower when the room temperature decreased below 33°C on the initial cooling cycle as predicted with the model for our setup. Calibration of the transducers was carefully tested at several temperatures within the range of 20 to 40°C . Room temperatures were measured using thermistor temperature sensors.

Our tests in the controlled temperature room confirmed the ability of the proposed model to predict the temperature effects for different geometries of the tension infiltrometer. We describe here the response of a single Mariotte tower to the imposed sinusoidal-like diurnal temperature variations (Fig. 4b). Figure 4a shows observed pressures in the air pocket, along with the imposed temperatures. As expected, the pressure varied in response to the changing temperature until bubbling started after about 0.45 d when the temperature dropped below T_i (i.e., when the meniscus reached its lowest position, and $P = P_i$). Air entry ceased only after the temperature started increasing again at 0.7 d. Since at this time the minimum temperature was reached and the maximum amount of air was stored in the Mariotte system, no more bubbling was observed for the remainder of the experiment. Notice that similar temperatures before and after bubbling (i.e., changes occurring in the mass of air) corresponding to different air pressures (e.g., compare pressures and temperatures at 0.3 and 1.0 d in Fig. 4). Equation [9] may be used to calculate the maximum change in pressure (ΔP) resulting from the imposed maximum temperature change (ΔT), in this case about 18.5°C (Fig. 4b). The model for our setup predicted a value of 11.2 cm for ΔP , which compared well with the measured change of 12.5 cm (Fig. 4a). The calculation was performed using the following parameter values for our experimental setup: $P_i = -18.0$ cm, $T_i = 20.0^{\circ}\text{C}$, $\Delta T = 18.5^{\circ}\text{C}$, $a_i = 5.0$ cm, and $\varepsilon = 0.33$ ($m = 0.25$).

IMPLICATIONS FOR IMPROVED TENSION INFILTRMETER DESIGN

Mariotte Tower

Equations [8] and [9] show that ΔP depends on the diameters of the Mariotte tower and the bubbling tube (through parameter ε), and on the initial height of the air pocket (a_i). In Fig. 5 we plotted calculated ΔP values as a function of ε for different values of a_i . The predicted changes in pressure correspond to a temperature increase of 10°C , with $T_i = 20^{\circ}\text{C}$ and $P_i = -100$ cm. For any a_i , ΔP decreases rapidly as the ratio ε increases, approaching a limiting value ΔP_{∞} (depending on a_i) for large value of ε . The shape of the curves in Fig. 5 reflects the fact that for large bubbling tubes (B ; i.e., with large ε values) the air pocket is relatively free to expand and therefore to release part of the pressure buildup, whereas small tubes restrict expansion of the air pocket. In the limit when $\varepsilon = 0$ (no tube in the Mariotte) no expansion is possible. The air pressure then builds up to a maximum (ΔP_{∞}), which is independent of a_i and can be obtained from Eq. [4] with $\Delta V = 0$. Hence, to contain the pressure buildup in the Mariotte tower in response to a tempera-

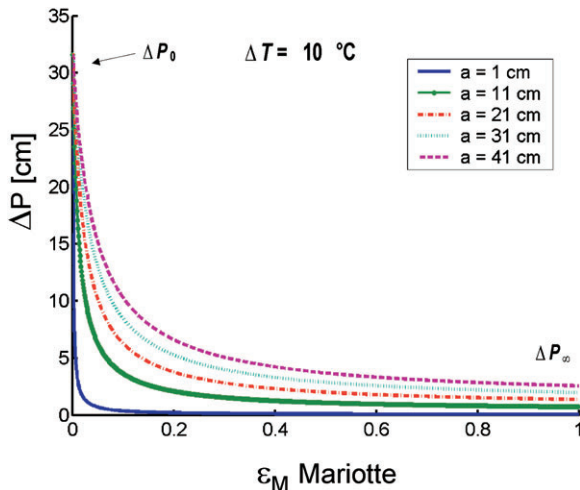


Fig. 5. Calculated pressure changes (ΔP) as a function of ϵ_M for different values of the initial height (a) of the air pocket.

ture increase, one simply needs to minimize a_i and maximize the ratio ϵ .

A simple but very effective alternative design for large-diameter bubbling tubes is illustrated in Fig. 2c. Air in this case enters the Mariotte tower through an external tube horizontally connected to the tower. Expansion of the air pocket with increasing temperature now does not affect the location of the water meniscus since $k = 0$, as shown in Fig. 2d, as long as water does not enter any vertical extension of the bubbling tube.

Tension Infiltrometer

In spite of the many parameters involved, the temperature model suggests several ways for improving the design of tension infiltrmeters. A primary concern should be the undesired overpressure ΔP_D at the disk; that is,

$$\Delta P_D = \Delta P_M + k_R \tag{18}$$

since excessive fluctuations in the imposed pressure head at the soil or rock surface may compromise the infiltration experiment. Large disturbances in the reservoir air pocket are also to be avoided because they produce noise in the cumulative infiltration data.

Our analysis shows that the larger the initial heights of the air pockets in the reservoir and the Mariotte towers (a_{Ri} and a_{Mi} in Fig. 3a), the more severe the pressure changes within the infiltrmometer system become. While a_{Mi} can usually be kept to a minimum when designing the Mariotte tower, a_{Ri} is less easily controlled since this parameter steadily increases during the infiltration process as the reservoir empties.

We also found that the response of the infiltrmometer system to temperature variations strongly depends on the cross-sectional areas of the two towers, as well as on the diameters of the bubbling tubes, Tubes B and C. In general, the larger the ratio $\epsilon_M = s_B/S_M$, the smaller the pressure variations. Figure 6 shows calculated pressure changes at different points in the system (solid lines) as a function of ϵ_M . For small ϵ_M values, the pressure increase in the Mariotte will eventually dominate the pressure increase in the reservoir, leading to bubbling as il-

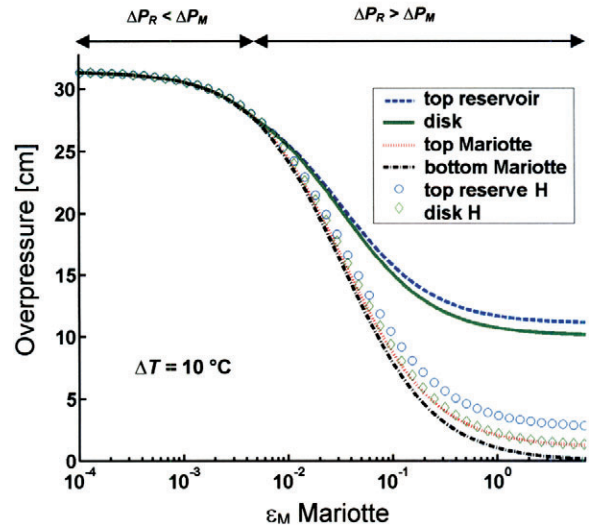


Fig. 6. Calculated overpressure as a function of the Mariotte ϵ_M at different locations within the infiltrmometer system.

lustrated in Fig. 3c. We note that when air bubbling occurs, the pressures at the disk and in the top parts of both the reservoir tower and the Mariotte tower are predicted to become equal. As for a single Mariotte tube, using external horizontal tubes is equivalent to imposing infinitely large ϵ_M ratios, thus ensuring minimum pressure buildup.

The choice of an appropriate value for the ratio $\epsilon_R = s_C/S_R$ is not as simple. The selection of a reservoir tower is generally governed by the desired accuracy in the infiltration rate measurements, which suggests using a diameter that is as small as possible. An increase in the diameter of Tube C connecting the Mariotte tower to the reservoir tower will increase ϵ_R , but at the same time will produce a larger V_{Mi} , which would have a negative effect by increasing the effective air pocket volume of the Mariotte tower. Our calculations indicate that the effects of variable temperatures on infiltrmometer pressure fluctuations can be minimized by adding a small section of horizontal tubing to the base of the reservoir, connected to Tube C. In this way the section of the tube can be kept small (thus minimizing V_{Mi}), while reducing the increase of the meniscus ($k_R = 0$). The temperature model indicates that this will reduce the pressure changes considerably. In Fig. 6 the calculated ΔP at the top of the reservoir (top reserve H) and at the disk (Disk H) are plotted against ϵ_M (open circles). Note that the overpressure at the disk is reduced from about 10 cm to <2 cm if Tube B is employed.

We also note that the temperature model in this study assumed that the system is closed to mass exchange, while the temperature varies (i.e., no air enters the Mariotte and no water leaves the reservoir tower). During actual infiltration experiments water will flow through the disk into the soil, which will lead to decreasing water levels in the reservoir tower while an equivalent volume of air will enter the system. This dynamic situation causes an expansion of the air pocket, for which the overpressure resulting from ΔT will be less severe than predicted with the equations derived here. Hence, temperature ef-

facts are a major concern only when the water level in the reservoir tower decreases very slowly compared with the rate at which temperature variations occur (e.g., because of rapidly changing temperature conditions and/or very low infiltration rates). One or both of these conditions may occur during experiments with fractured rocks, in which case proper tension infiltrometer design becomes very important (e.g., Castiglione et al., 2005).

CONCLUSIONS

Our main objective was to develop an analytical model that shows explicitly the effects of temperature on tension infiltrometer performance, and how to use the model to design an improved infiltrometer that minimizes the temperature effects. The effects can be significant under certain environmental conditions, especially when the infiltration rate is very low, such as for experiments with very fine-textured soils or fractured rock formations. We have shown that the proposed model based on the ideal gas law can be used to predict the distribution of pressures in a static infiltrometer system. While not as rigorous as a more comprehensive analysis for transient conditions involving infiltration, the static analysis nevertheless provides enough information to significantly improve the design of an infiltrometer that is far less temperature sensitive than most or all tension infiltrometers currently available commercially. Our ultimate goal was to design an infiltrometer that can be used to characterize the flow regime of fractured rock and other low permeability media (e.g., landfill caps and clay liners) requiring long equilibration times. Although temperature effects may not be eliminated completely in many applications, our study indicates that tension infiltrometers can be designed that are far less sensitive to temperature variations.

We also showed that response of the tension infiltrometer system depends greatly on its geometry through a large number of parameters. Some of these parameters cannot be controlled, and/or must comply with other requirements of the device, whereas other parameters may be optimized to minimize pressure variations throughout the system. We believe that the proposed temperature model represents a relatively simple, yet useful tool to investigate the effects of the different parameters involved, thus potentially providing guidance for additional design improvements for tension infiltrometers in the future.

ACKNOWLEDGMENTS

This study was based on work supported in part by SAHRA (Sustainability of semi-Arid Hydrology and Riparian Areas) under the STC Program of the National Science Foundation, Agreement no. EAR-9876800.

REFERENCES

- Ankeny, M.D., T.C. Kaspar, and R. Horton. 1988. Design for an automated tension infiltrometer. *Soil Sci. Soc. Am. J.* 52:893–895.
- Bagarello, V., M. Iovino, and G. Tusa. 2000. Factors affecting measurement of the near-saturated soil hydraulic conductivity. *Soil Sci. Soc. Am. J.* 64:1203–1210.
- Butters, G.L., and G.E. Cardon. 1998. Temperature effects on air-pocket tensiometers. *Soil Sci.* 163:677–685.
- Castiglione, P., P.J. Shouse, B. Mohanty, D. Hudson, and M.Th. van Genuchten. 2005. Improved infiltrometers for measuring low fluid flow rates in unsaturated fractured rock. Available at www.vadosezonejournal.org. *Vadose Zone J.* 4 (this issue).
- Clothier, B.E., and I. White. 1981. Measurement of sorptivity and soil water diffusivity in the field. *Soil Sci. Soc. Am. J.* 45:241–245.
- Jarvis, N.J., and I. Messing. 1995. Near-saturated hydraulic conductivity in soils of contrasting texture measured by tension infiltrometers. *Soil Sci. Soc. Am. J.* 59:27–34.
- Lin, H.S., and K.J. McInnes. 1995. Water flow in clay soil beneath a tension infiltrometer. *Soil Sci.* 159:375–382.
- Mohanty, B.P., R.S. Bowman, J.M.H. Hendrickx, and M.Th. van Genuchten. 1997. New piecewise-continuous hydraulic functions for modeling preferential flow in an intermittent flood-irrigated field. *Water Resour. Res.* 33:2049–2063.
- Mohanty, B.P., R. Horton, and M.D. Ankeny. 1996. Infiltration and macroporosity under a row crop agricultural field in a glacial till soil. *Soil Sci.* 161:205–213.
- Perroux, K.M., and I. White. 1988. Designs for disc permeameters. *Soil Sci. Soc. Am. J.* 52:1205–1214.
- Richards, L.A., M.B. Russell, and O.R. Neal. 1937. Further developments on apparatus for field moisture studies. *Soil Sci. Soc. Am. Proc.* 2:55–64.
- Schwartz, R.C., and S.R. Evett. 2002. Estimating hydraulic properties of a fine-textured soil using a disc infiltrometer. *Soil Sci. Soc. Am. J.* 66:1409–1423.
- Simunek, J., D. Wang, P.J. Shouse, and M.Th. van Genuchten. 1998. Analysis of field tension disk infiltrometer data by parameters estimation. *Int. Agrophys.* 12:167–180.
- Vandervaere, J.P., M. Vauclin, and D.E. Elrick. 2000. Transient flow from tension infiltrometers: II. Four methods to determine sorptivity and conductivity. *Soil Sci. Soc. Am. J.* 64:1272–1284.
- Warrick, A.W., P.J. Wierenga, M.H. Young, and S.A. Musil. 1998. Diurnal fluctuations of tensiometric readings due to surface temperature changes. *Water Resour. Res.* 34:2863–2869.
- Watson, K.W., and R.J. Luxmoore. 1986. Estimating macroporosity in a forested watershed by use of a tension infiltrometer. *Soil Sci. Soc. Am. J.* 50:578–582.
- Wilson, G.V., and R.J. Luxmoore. 1988. Infiltration, macroporosity, and mesoporosity distributions on two forested watersheds. *Soil Sci. Soc. Am. J.* 52:329–335.
- Wooding, R.A. 1968. Steady infiltration from large shallow circular pond. *Water Resour. Res.* 4:1259–1273.